Catal Lett (2008) 122:228–237
DOI 10.1007/s10562-008-9432-6

Optimization of Ethylene Production via Catalytic Partial Oxidation of Ethane on Pt–$LaMnO_3$ Catalyst

S. Cimino · F. Donsì · G. Russo · D. Sanfilippo

Received: 21 December 2007 / Accepted: 7 February 2008 / Published online: 26 February 2008
© Springer Science+Business Media, LLC 2008

Abstract A novel catalyst formulation (Pt–$LaMnO_3$) was recently developed and disclosed for ethylene production via the catalytic partial oxidation of ethane at short contact time. In this paper we report results of the extensive experimental campaign performed on the Pt–$LaMnO_3$ system for the tuning and optimization of process parameters, which, in turn, shed light on the effect of the main variables controlling overall performance. The novel catalytic system under optimized operating conditions was capable of performances better than state-of-the art systems, with ethylene yields exceeding 65% while preserving selectivities above 80% under self-sustained operation, by adding H_2 as a sacrificial fuel in a simple reactor configuration, thus suggesting to reconsider the economical viability of ethylene production by ethane CPO at short contact time.

Keywords Oxidative dehydrogenation · Olefin production · Catalytic partial oxidation · Short contact time reactors · Pt Perovskite · Ethane

1 Introduction

Olefins have become the building blocks for the production of polymers and consequently for the manufacture of an impressive number of commodities and specialties for daily use [1].

Ethylene production by the endothermic steam cracking of light hydrocarbons is currently one of the most energy and capital intensive processes in the petrochemical industry [2]. Since the pioneering work of Huff and Schmidt [3], the selective oxidative dehydrogenation (ODH) of ethane to ethylene over Pt-based structured catalysts operated at short contact time has attracted some interest as a possible alternative route to steam cracking [4–6].

This technology relies on the combination of three different reaction paths of the paraffinic hydrocarbons: the catalytic partial oxidation (CPO) with (pure) oxygen, which is a self-sustaining autothermal process, the oxidative dehydrogenation (ODH), in competition with CPO, and the thermal cracking at high temperature, which is driven by the in situ combustion of part of the feed [7, 8].

Due to a simpler reactor system (no need for large external furnaces) and fewer fractionation columns, estimated investment cost for the ethane CPO process is about 20–25% lower than for the corresponding ethane steam cracker. On the other hand, estimated production costs are somewhat higher (10–15%), mainly due to the additional cost of making or purchasing oxygen [9, 10].

In particular, an economic analysis by Shell concluded that ethane CPO might be marginally more attractive than ethane steam cracking at comparable ethylene yields (48–50 mol% on a single pass, with 80–85% carbon selectivity), which, however, was considered to be a very optimistic assumption with state of the art catalysts. It was also reported economic attractiveness of catalytic partial oxidation process is highly sensitive even on small yield variations [11].

Until recently, platinum emerged as the most active catalyst for ethylene formation from ethane [3, 4, 12, 13].

S. Cimino (✉) · G. Russo
Istituto Ricerche sulla Combustione, CNR Napoli,
P.le V. Tecchio 80, Napoli 80125, Italy
e-mail: cimino@irc.cnr.it; stcimino@unina.it

F. Donsì
Dipartimento Ingegneria Chimica ed Alimentare,
Università di Salerno, Fisciano (SA), Italy

D. Sanfilippo
Snamprogetti Spa, San Donato Milanese, Italy

Furthermore, doping Pt with tin or copper resulted in improved performance for ethane ODH, with a significant increase in ethylene yield [14], which was even greater as a result of H_2 addition as sacrificial fuel [7, 15]. Nevertheless, such catalysts were afflicted by the high cost of Pt and volatility of the active phase (Pt, Sn, Cu). Despite these results, efforts to obtain ethylene yields higher than that for steam cracking have been elusive [16].

Requirements for higher performance led to the development of a novel catalyst formulation (Pt–$LaMnO_3$) [17], with a multi-layered structure consisting Pt deposited onto a layer of $LaMnO_3$ perovskite supported over monolithic structures. The deposition of Pt onto $LaMnO_3$ phase results in a better dispersion of the noble metal, which is hence required in small amounts, and can be effectively stabilized at the operation temperature. Moreover, due to the strong interaction between two active phases, Pt and $LaMnO_3$, the catalyst performance is greatly enhanced, resulting in higher ethylene selectivity and higher conversion with respect to either Pt or $LaMnO_3$ alone [17].

In this paper we report results of the extensive experimental campaign performed on the Pt–$LaMnO_3$ system for the tuning and optimization of process parameters, which, in turn, shed light on the effect of the main variables controlling overall performance.

In addition, through a simplified homogeneous model, we try to highlight some key features of the process and the margins for further improving the reactor performance.

2 Experimental

2.1 Catalyst Preparation

The multilayered catalyst structure consists of a La_2O_3-stabilized γ-Al_2O_3 washcoat layer, anchored by a dip-coating procedure [18] on cordierite substrates with honeycomb morphology (square channels) and channel density of 600 cpsi, provided by NGK. $LaMnO_3$ perovskite is dispersed onto the washcoat layer by repeated cycles of co-impregnation with a solution of the precursor salts, as previously described [19]. Finally Pt is added to the catalysts by impregnation of the coated monolith with a diluted H_2PtCl_6 solution. The catalysts were calcined in air at 800 °C after the deposition of each layer and at 1,000 °C for 3 h before testing.

2.2 Experimental Set-up and Procedure

The catalytic monolith, in the shape of disk of ~18 mm diameter and 12 mm long, is stacked between two inert mullite foam monoliths (45 ppi, same dimensions) as radiation shields, whereas a further SiC foam monolith (10 ppi) is placed as a static mixer before the stack, as shown in Fig. 1.

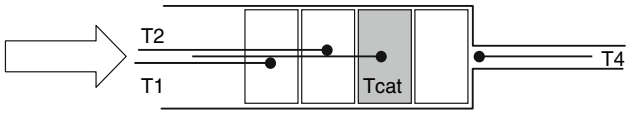

Fig. 1 Schematic representation of catalytic reactor set-up

The stack of monoliths is placed in a quartz reactor (i.d. 20 mm) externally heated by an electric furnace to ensure desired preheating. The post-reaction zone is specifically designed with a rapidly decreasing passage section in order to reduce the residence time of reacted gas at high temperature and stop undesired secondary reactions (condensation), which may significantly affect process selectivity.

Three K-type thermocouples ($d = 0.5$ mm) are placed respectively in the central part of the mixer (T1), in the front radiation shield (T2, upstream of the catalyst), in the middle of the central channel of the catalyst (Tcat); a fourth thermocouple (T4, K-type with $d = 1$ mm) is placed downstream of the back heat shield to measure the gas exit temperature (Fig. 1).

High-purity gases calibrated via Brooks 5850-series mass-flow controllers are pre-mixed and fed to the reactor at gas hourly space velocity (GHSV) comprised between 30,000 and to 80,000 h^{-1} (standard conditions on the basis of monolith volume) corresponding to residence times as low as 14 ms at the average reactor temperature of 900 °C. Reactor pressure is always kept at 1.2 atm, and feed composition is always above the upper flammability limit at room temperature.

Reaction tests were undertaken at varying C_2H_6/O_2 ratio in the range 1.5–2.25 and H_2/O_2 ratio in the range 0–4, O_2 flow rates between 19 and 35 slph, which in turn controls GHSV and heat produced, while furnace temperature was varied between 250 and 550 °C.

Product gases pass through a condenser and a $CaCl_2$ trap to selectively remove water, prior to splitting to a ABB continuous analyzer, employed to measure concentrations of H_2 (Caldos17), CO, CO_2, and CH_4 (Uras14), and to an on line gas chromatograph equipped with molecular sieve and Poraplot Q columns and TCD + FID detectors to measure C_2H_6, C_2H_4, C_2H_2, CH_4, N_2, O_2, CO, CO_2, and other eventual hydrocarbons up to C_4. The carbon balance was always closed within 2% using N_2 (5–10 vol.%) as internal standard.

2.3 Reactor Model

As a first approximation, the system was modeled as a plug-flow reactor. The ideal Reynolds number (<100) and the very high length-to-diameter ratio specific for the

channel geometry suggest that axial dispersion is extremely low, while on the other side, since the extent of radial dispersion is rather small, significant radial gradients should be expected in the honeycomb monoliths used in the experimental campaign. These considerations led to the conclusion that the validity of the plug-flow model is limited to preliminary estimates of the contribution of homogeneous reactions.

The mass equations for a plug-flow reactor can be written as

$$\rho \vartheta_2 A \frac{d\omega_i}{dz} + \omega_i a_i \sum_{\text{gas}}^{K_g} \dot{g}_i W_i = W_i(\dot{g}_i a_i + \dot{\omega}_i A) \quad (1)$$

$$\rho \vartheta_x = \frac{d\omega_i}{dz} = W_i \dot{\omega}_i \quad (2)$$

where a_i, internal surface area of channel per unit length, m^2/m; ρ, density, kg/m^3; υ_z, axial velocity, m/s; ω_i, mass fraction of species i; A, channel cross-sectional area, m^2; z, axial coordinate, m; K_g, number of gas-phase species; $\dot{g}_i$, production rate of species i by all surface reactions, mol/(m^2 s); W_i, molecular weight of species i, kg/mol; $\dot{\omega}_i$, production rate of species i by all homogeneous reactions, mol/(m^3 s).

Numerical simulations were performed using the Chemkin PLUG code [21] for a single channel of 1 mm diameter and inlet velocity of 0.1 m/s. Simulations were carried out under isothermal conditions, varying temperature level between 800 and 1,050 °C. The inlet pressure was always 1.2 atm, dilution was 1 vol% N_2 for internal standard and the C_2H_6/H_2O ratio was always set to 1.0. Even if the honeycomb reactor is only 12 mm long (plus 12 mm of the back heat shield monolith), the total length modeled was virtually increased in order to capture any gas-phase chemistry occurring towards equilibrium; however, final gas composition was achieved within 20 mm for any $T \geq 900$ °C.

3 Results and Discussion

3.1 Screening of the Operating Parameters of the Pt–$LaMnO_3$ Catalytic Systems

Each single operative parameter plays a not easily predictable role on the performance of the partial oxidation of ethane at short contact time, since the effects on process conversion and selectivity are indirect, strictly interconnected and involve (among others) variations of residence times and temperature profiles in the reactor, the adiabaticity of the system and the exothermicity of the reacting mixture. Neglecting the small amount of N_2 added as an internal standard for product analysis and quantification, the experimental set was conducted with 4 degrees of freedom, by independently varying the feed flow rates of ethane, oxygen, and hydrogen and the (preheating) temperature of the system by means of the external furnace.

Table 1 summarizes the experimental data set, which was preliminary performed on the novel Pt–$LaMnO_3$ catalyst.

Since it was not possible to design an experimental matrix, which would decouple all the single effects for each parameter, a statistical approach was implemented by means of a simple linearized model.

The last line in Table 1 reports the arithmetic average for each variable (independent and observed) across the whole set of data $\bar{x}_i$.

The results in terms of ethane conversion (C) and total selectivity to ethylene + acetylene (S) were linearized around their average values ($\bar{C}$, $\bar{S}$) by applying the following equations:

$$\frac{\Delta C}{\bar{C}} = b_1 \frac{\Delta x_1}{\bar{x}_1} + b_2 \frac{\Delta x_2}{\bar{x}_2} + b_3 \frac{\Delta x_3}{\bar{x}_3} + b_4 \frac{\Delta x_4}{\bar{x}_4} \quad (3)$$

$$\frac{\Delta S}{\bar{S}} = a_1 \frac{\Delta x_1}{\bar{x}_1} + a_2 \frac{\Delta x_2}{\bar{x}_2} + a_3 \frac{\Delta x_3}{\bar{x}_3} + a_4 \frac{\Delta x_4}{\bar{x}_4} \quad (4)$$

where $\bar{x}_i$ and Δx_i represent respectively the average value and the difference from it of each of the four independent variables x_i. In particular, the arbitrary set of four independent variables which was used to perform data regression, comprised the C_2H_6/O_2 (indicated by C_2/O_2) and H_2/O_2 feed ratios, the total gas hourly space velocity (GHSV) and the preheating level (indicated by Tpre) as measured by the temperature of the gas approaching the catalytic monolith (T1 in Fig. 1).

The coefficients a_i and b_i, which are obtained from the experimental data regression, represent the percentage gain or loss in conversion and selectivity with respect to their own averages as a consequence of the variation of each independent variable.

The parity plot and the specific coefficients obtained by the linear regression are reported in Fig. 2a, b. The linearized expressions (3 and 4) are able to accurately reproduce all the experimental data with regard to both ethane conversion and total selectivity to unsaturated hydrocarbons, such as C_2H_4 and C_2H_2 (unsaturated C2). In fact all examined process variables show a contrasting effect on the catalytic performance, since an enhancement in conversion is always paid by a reduction in the overall process selectivity.

From Fig. 2b it is evident that ethane conversion mostly depends on C_2/O_2, for which it shows the highest negative sensitivity. In contrast, it is only slightly decreased when H_2/O_2 is increased and is even less reduced for an increment of the GHSV. On the other hand, a higher preheating of reactants enhances C_2H_6 conversion.

Table 1 Experimental conditions and results of preliminary tests conducted on Pt–$LaMnO_3$ catalyst

Feed								Results						Temperatures			
C_2H_6/O_2	H_2/O_2	Oven (°C)	GHSV (h^{-1})	N_2 (slph)	O_2 (slph)	C_2H_6 (slph)	H_2 (slph)	Conv. (%)	Sel. C_2H_4 (%)	Sel. tot C_2 (%)	C_2 yield Tot (%)	C bal.	H bal.	T1 (°C)	T2 (°C)	Tcat (°C)	T4 (°C)
1.50	0.0	250	3.59E + 04	7.5	27.0	40.5	0.0	95.3	49.1	53.7	51.1	−0.1	−1.9	266	364	1,015	743
1.50	0.0	350	3.59E + 04	7.5	27.0	40.5	0.0	96.5	46.1	51.2	49.4	−1.3	−2.6	345	457	1,035	771
1.50	0.0	400	3.59E + 04	7.5	27.0	40.5	0.0	97.0	45.4	50.9	49.4	0.6	−1.8	456	668	1,041	770
1.50	1.0	250	4.89E + 04	7.5	27.0	40.5	27.0	93.6	55.7	60.4	56.5	−0.8	−2.1	296	415	1,013	763
1.50	2.0	250	6.18E + 04	7.5	27.0	40.5	54.0	91.9	61.2	65.7	60.4	−0.7	−0.3	291	397	1,005	778
1.50	2.5	250	6.83E + 04	7.5	27.0	40.5	67.5	90.6	65.4	69.9	63.3	−1.2	0.6	278	375	998	783
1.75	0.0	350	3.59E + 04	7.5	24.5	43.0	0.0	90.0	60.7	64.0	57.6	−1.4	−2.7	312	412	973	741
1.75	0.0	350	3.59E + 04	7.5	24.5	43.0	0.0	88.8	59.1	61.6	54.7	−1.4	−2.5	297	376	963	740
1.75	0.0	400	3.59E + 04	7.5	24.5	43.0	0.0	90.8	58.3	61.4	55.7	−2.0	−3.3	357	430	979	754
1.75	0.5	500	4.18E + 04	7.5	24.5	43.0	12.3	91.7	58.8	62.6	57.3	−1.7	−3.0	462	599	1,002	780
1.75	1.0	350	4.77E + 04	7.5	24.5	43.0	24.5	87.2	65.9	69.0	60.2	−0.3	−1.7	347	476	973	755
1.75	1.0	500	4.77E + 04	7.5	24.5	43.0	24.5	90.4	62.3	65.9	59.6	−0.4	−1.9	475	613	997	786
1.75	2.5	250	6.53E + 04	7.5	24.5	43.0	61.4	80.1	74.0	76.4	61.2	−1.6	−1.6	264	352	950	758
1.75	2.5	350	6.53E + 04	7.5	24.5	43.0	61.4	82.8	74.4	77.3	64.0	0.6	−0.1	337	453	964	770
1.75	2.5	500	6.53E + 04	7.5	24.5	43.0	61.4	86.8	69.8	73.2	63.6	−1.2	−0.9	457	586	985	797
1.75	3.0	350	7.12E + 04	7.5	24.5	43.0	73.6	81.5	73.5	76.1	62.0	−1.0	−1.0	323	436	958	772
1.75	3.0	500	7.12E + 04	7.5	24.5	43.0	73.6	84.8	73.3	76.4	64.8	0.0	0.8	443	565	979	797
1.75	3.0	500	7.12E + 04	7.5	24.6	43.0	73.6	83.2	75.2	78.5	65.4	−0.1	1.3	444	590	1,002	779
1.75	4.0	500	8.29E + 04	7.5	24.6	43.0	98.0	77.2	77.8	80.4	62.1	−1.7	−0.7	448	692	987	793
1.90	3.0	500	8.39E + 04	10.0	28.0	53.2	84.0	73.0	82.2	84.5	61.7	1.5	0.2	407	615	971	791
1.90	3.0	500	8.96E + 04	10.0	30.0	57.0	90.0	72.9	82.3	84.5	61.6	1.3	0.2	385	565	971	796
2.00	0.0	350	3.59E + 04	7.5	22.5	45.0	0.0	79.9	67.0	68.8	55.0	−2.0	−2.8	295	386	928	721
2.00	0.0	350	3.59E + 04	7.5	22.5	45.0	0.0	77.2	66.1	67.5	52.2	−2.2	−3.3	276	348	921	716
2.00	0.0	400	3.59E + 04	7.5	22.5	45.0	0.0	80.5	65.0	66.7	53.7	−3.2	−3.9	331	397	932	732
2.00	2.5	500	8.38E + 04	10.0	30.0	60.0	75.0	70.5	83.3	85.3	60.1	2.0	0.1	382	542	964	789
2.00	3.0	500	6.53E + 04	7.5	21.5	43.0	64.4	70.0	80.4	82.0	57.4	−0.4	−0.6	465	627	964	756
2.00	3.0	500	7.41E + 04	7.5	24.6	49.1	73.6	69.9	83.6	85.5	59.8	2.4	1.1	431	594	971	765
2.00	3.0	500	8.53E + 04	10.0	28.0	56.0	84.0	70.3	84.3	86.5	60.8	2.4	0.1	410	583	961	789
2.00	3.0	500	9.10E + 04	10.0	30.0	60.0	90.0	68.6	84.2	86.2	59.1	1.5	−0.1	370	528	960	790
2.00	3.4	500	6.97E + 04	7.5	21.5	43.0	73.6	70.1	79.9	81.4	57.1	−1.3	−0.8	471	633	965	760

Table 1 continued

Feed							Results					Temperatures			
C_2H_6/O_2	H_2/O_2	Oven (°C)	GHSV (h^{-1})	N_2 (slph)	O_2 (slph)	C_2H_6 (slph)	H_2 (slph)	Conv. (%)	Sel. C_2H_4 (%)	Sel. tot C_2 (%)	C_2 yield Tot (%)	C bal.	H bal.	T1 (°C)	T2 (°C)	Tcat (°C)	T4 (°C)
2.25	0.0	350	3.59E + 04	7.5	20.8	46.7	0.0	68.2	71.6	72.7	49.6	0.1	−1.1	283	360	902	706
2.25	3.0	500	6.08E + 04	7.5	19.1	43.0	57.3	59.2	82.7	83.9	49.7	−0.6	−1.6	469	627	941	738
2.25	3.0	500	7.71E + 04	7.5	24.6	55.2	73.6	60.6	87.2	88.5	53.6	2.4	0.2	400	550	949	757
2.25	3.0	500	$^{8.86E+04}$	10.0	28.0	63.0	84.0	59.0	87.6	89.1	52.5	1.9	−0.5	358	510	938	776
2.25	3.9	500	6.86E + 04	7.5	19.1	43.0	73.6	56.7	84.6	85.7	48.6	−0.8	−0.9	^{452}	^{616}	^{941}	^{743}
Mean value																	
1.85	1.87	417	6.0E + 0	7.9	25.0	46.0	46.7	79.6	70.8	73.5	57.4	−0.3	−1.1	374	507	971	764

This data set was used for the statistical analysis

Regarding overall process selectivity, the parameter showing the highest effect is the feed ratio C_2/O_2, followed by GHSV: in both cases, an increment of the parameter causes an increase of selectivity. Instead, variations from their corresponding average values of the H_2/O_2 and Tpre marginally affect the process selectivity with opposite trends: the increase of H_2/O_2 is beneficial to selectivity, while high preheating has a reducing effect.

In fact, when all the experimental values of ethane conversion and total selectivity to unsaturated C2 are plotted as a function of the corresponding temperatures measured in the catalytic reactor, a strong correlation was made evident between performance and catalyst temperature, as shown in Fig. 2c. Ethane conversion always increases at increasing catalyst temperature, with a linear trend once fixed the preheat temperature, whereas selectivity slightly decreases at low Tcat and more rapidly above 980 °C: the optimal catalyst temperature for maximum process yield is around this value. In contrast, the other temperatures measured upstream and downstream of the catalytic layer are not in a simple correlation with the values of overall conversion and selectivity.

Bodke et al. showed that, with the exception of feed composition, the effects of preheat, dilution, and higher pressure on the ethane ODH performance of Pt–Sn catalysts all appear to be explainable through the temperature changes they induce in the catalytic reactor. Thus preheat, absence of dilution, and higher pressures all tend to increase the catalyst temperature, which, in turn, increases ethane conversion while lowering selectivity [7].

Accordingly to our results, over these catalysts it was found that, at increasing C_2/O_2, ethane conversion decreases while ethylene selectivity increases, corresponding to a decrease in reactor temperature [18].

From the point of view of process optimization, a summary of the influence of each operative variable is depicted in Fig. 3, where in the conversion-selectivity plane the predicted catalytic performance is back calculated from equations [3, 4] by changing each variable separately. The coordinates of the central point in the graph are represented by the values of the average conversion and selectivity ($\bar{C} = 79.6\%$, $\bar{S} = 73.5\%$) around which data were linearized; lines departing from it show the effect of variation of each single variable, while maintaining constant the values of all the remaining variables. Both incremental and decremental steps of 10% with respect to the average value are represented by the symbols along the lines corresponding to any parameters in Fig. 3.

Increasing process severity by reducing C_2/O_2 feed ratio improves the total yield per pass but at the expense of selectivity which rapidly drops below 70% at $C_2/O_2 = 1.5$. Indeed, considering that the cost of oxygen would have the largest impact on the economics of the process and that the

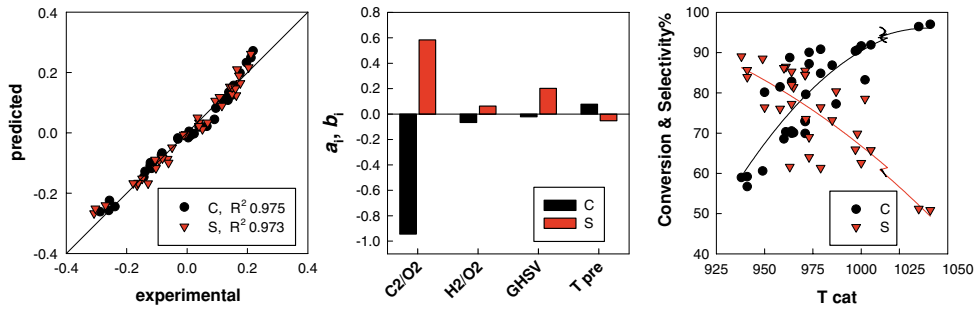

Fig. 2 (**a**) Parity plot for ethane conversion (*C*) and total selectivity to unsaturated C2 (*S*), obtained by the linear regression around the average experimental values. (**b**) Sensitivity coefficients for each independent variable with respect to process conversion and total selectivity. (**c**) Dependence of experimental *C* and *S* data on measured catalyst temperature

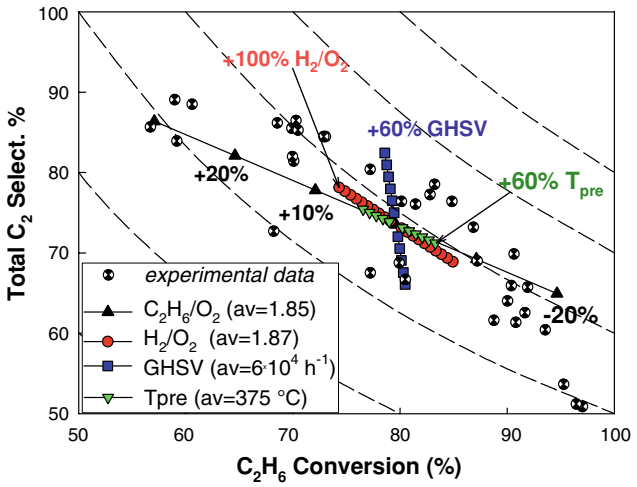

Fig. 3 Star diagram of total selectivity and conversion, including the effect on the catalytic system of the percentage increase (or decrease) of any independent variable around its average value (reported in the legend)

unconverted ethane maybe separated and recycled back to the reactor, an effective optimization strategy requires preserving high selectivity per pass (at least 80% on a molar basis). With such a constraint in mind, it follows that optimal C_2/O_2 should not fall below 2, the stoichiometric value for the oxidative dehydrogenation of ethane to ethylene [11].

H_2 addition as sacrificial fuel has been demonstrated to be an effective strategy to reduce C_2H_6 consumption for undesired side reactions towards oxidized CO_x species. Indeed H_2 rather than C_2H_6 is preferentially oxidized on Pt based catalysts with the molecular oxygen of the feed [7]. Such circumstance has two major implications: (i) more ethane is free to react to form C_2H_4; (ii) a better thermal management of the self-sustained catalytic reaction is achieved due to the larger net combustion heat per mole of oxygen liberated by H_2 rather than C_2H_6 (respectively 484 vs. 408 kJ/mol$_{O_2}$). This is particularly true if one considers that under fuel rich conditions ethane is not fully oxidized even on total oxidation catalyst such as $LaMnO_3$ [19] or Pt–$LaMnO_3$ [17]. In turn, H_2 addition allows operating the catalytic reactor at the same self-sustained temperature level but with a lower oxygen consumption, higher ethylene selectivity and virtually unchanged yield. Optimal H_2/O_2 feed ratio always falls between 2 to 3, i.e. above the stoichiometric value for H_2 combustion: the excess of H_2 is useful to further increase the oxygen selectivity to form water, since at the high catalyst operating temperature, under fuel rich conditions, the oxidation of ethane is fast enough to compete with that of H_2.

From Fig. 3 it is also evident that by increasing the space velocity it is possible to obtain a remarkable improvement in the process selectivity at the expense of a small reduction in conversion. This effect is not surprising if one considers that the catalytic process is not kinetically limited, therefore a reduction in the contact time over the catalyst even below 1 ms does not affect negatively ethane conversion. On the other hand, improved mass transfer coefficients related to higher flow rates and, most of all, a higher degree of adiabaticity for the relatively small lab scale rig which is attained when the catalytic reactor is operated at higher specific power, may even enhance ethane conversion.

The improvement in selectivity is probably related to the reduction of the residence time in the gas phase within the catalyst module and beyond it, which in turn affects the coupling of hetero-homogeneous reactions: in particular it is helpful to minimize the undesired formation of higher hydrocarbons (C4+) by condensation reactions which consume ethylene just formed and entail a further problem (and cost) for the downstream separation [8].

In our experimentation the rapid quenching of hot products from reaction zone was accomplished by a strong reduction in the flow section of the exit reactor zone, which was also exposed at ambient temperature and helped to maintain the C-atom selectivity to C3+ hydrocarbons always below 3–4%.

Finally, by increasing the preheat temperature, ethane conversion is enhanced, while the corresponding reduction in ethylene selectivity occurs at lower extent. It follows that preheating may result in an efficient strategy to compensate the reduction of conversion for instance due to a larger C_2/O_2 or GHSV.

In fact, due to the existence of a well defined catalyst temperature window for optimal operation between 960 and 1,000 °C already shown in Fig. 2, it turns out a high preheat temperature is useful to supply part of the heat required to the dehydrogenation reaction, advantageously reducing the amount of oxygen employed in the feed stream, which translates directly into economic savings.

3.2 Optimization of the Operating Conditions

On the basis of the results of the statistical analysis, a supplemental experimental campaign was conducted with the aim of optimizing the performance of the Pt–$LaMnO_3$ catalyst for the partial oxidation of ethane in terms of maximization of ethylene yield and selectivity. In particular, while the C_2/O_2 feed ratio was varied in the range 1.75–2.25, the study of the effect of other operating parameters suggested using the largest possible GHSV due to the positive impact on selectivity, which sensibly exceeds the corresponding decrease of ethane conversion. At the same time, conversion can be sustained by further increasing the preheating of reactants, while keeping the H_2/O_2 at values ≥ 2, in order to preserve a high selectivity to olefins. Due to limitations of the experimental rig, maximum gas preheating achieved was 475 °C (corresponding to a furnace set point of 550 °C), and the maximum GHSV was limited to $1.0 \times 10^5\ h^{-1}$ at standard conditions (corresponding to 3.5 SLPM). In addition, some runs were also carried out without N_2 dilution, in order to avoid any dilution effect and increase catalyst temperature. In such case, N_2 was added downstream of the reactor as an internal standard for the analysis of the products.

Experimental results of optimization of the operative conditions are reported in Fig. 4, where they are directly compared with the best literature results reported on state of the art Pt–Sn catalysts [7, 22]. In fact the data set from [7] were obtained on foam monoliths (45 ppi) operated autothermally with a feed of $C_2/O_2 = 2$ and H_2/O_2 variable in the range 1–3 [22], whereas those from were obtained on coated honeycomb monoliths (400 cpsi) at fixed feed composition ($C_2H_6/O_2/H_2 = 2/1/3$) and variable external preheating up to very high levels (850 °C).

As shown in Fig. 4, the best results obtained over the novel Pt–$LaMnO_3$ catalyst after optimization of process parameters with the help of the statistical analysis are significantly better than the previous results: a total molar yield to ethylene and acetylene in excess of 66% per pass was obtained, in correspondence to a C-atom selectivity to ethylene and ethane conversion both above 80%.

Interestingly, the reported data also highlight the high reproducibility of the performance of the catalytic system used and its thermal stability. Especially in the field of operation of greater interest for industrial application, that is with yield above 60% and selectivity above 80%, excellent results were obtained with several combinations of C_2/O_2, H_2/O_2, GHSV and preheat.

Noticeably, the best data obtained follow a single line in the conversion-selectivity diagram.

A direct comparison of the products distribution obtained over the two catalytic systems is also reported in Fig. 4. It appears that for both systems all the major species follow the same qualitative trend as a function of ethane conversion, whose increment is always accompanied by a corresponding increase of C-atom selectivity to CO, CH_4, C_2H_2, and CO_2 and, consequently, a reduction in C_2H_4 selectivity. Pt–$LaMnO_3$ monolith performs better in terms of ethylene selectivity than the best Pt–Sn catalytic systems known in the art, at any conversion level up to 85%, while above such value, its performance is aligned with those of Pt–Sn.

Characteristic plots of selectivity to C_2H_2 and CH_4 are superimposed for the two catalysts, suggesting a similar role played by the catalytic surfaces in their formation, which largely derives from the thermal dehydrogenation and cracking of ethane. On the other hand some differences may be noticed between the two catalysts in the C-selectivity to CO and CO_2: Pt–$LaMnO_3$ produces slightly lower amounts of CO than Pt–Sn in the zone of maximum ethylene yields, around 80% ethane conversion. At the same time the CO_2 selectivity is constantly higher on the novel catalyst, with an absolute value limited at around 1%, most probably due to the occurrence of the (endothermic) reverse water gas shift reaction $CO_2 + H_2 (CO + H_2O$ in the exit gas favored by high temperatures and the large excess H_2.

Therefore Pt–$LaMnO_3$ displays an overall improved selectivity to total oxidation of carbon species with respect to the Pt–Sn counterpart, which produces more partial oxidation products. In turn this effect helps to realize a better heat management, reducing the amount of C_2H_6 consumed to produce heat inside the catalytic reactor, or, in other words, reducing the amount of oxygen required in the feed.

The plots of O-atom selectivity to H_2O over the two catalysts also reveal that Pt–$LaMnO_3$ ensures a significantly enhanced formation of water instead of CO_x, particularly for medium to high process severity, i.e. in the high catalyst temperature range. This circumstance suggests a better effectiveness of H_2 addition as sacrificial fuel, since it is oxidized with higher selectivity with respect to

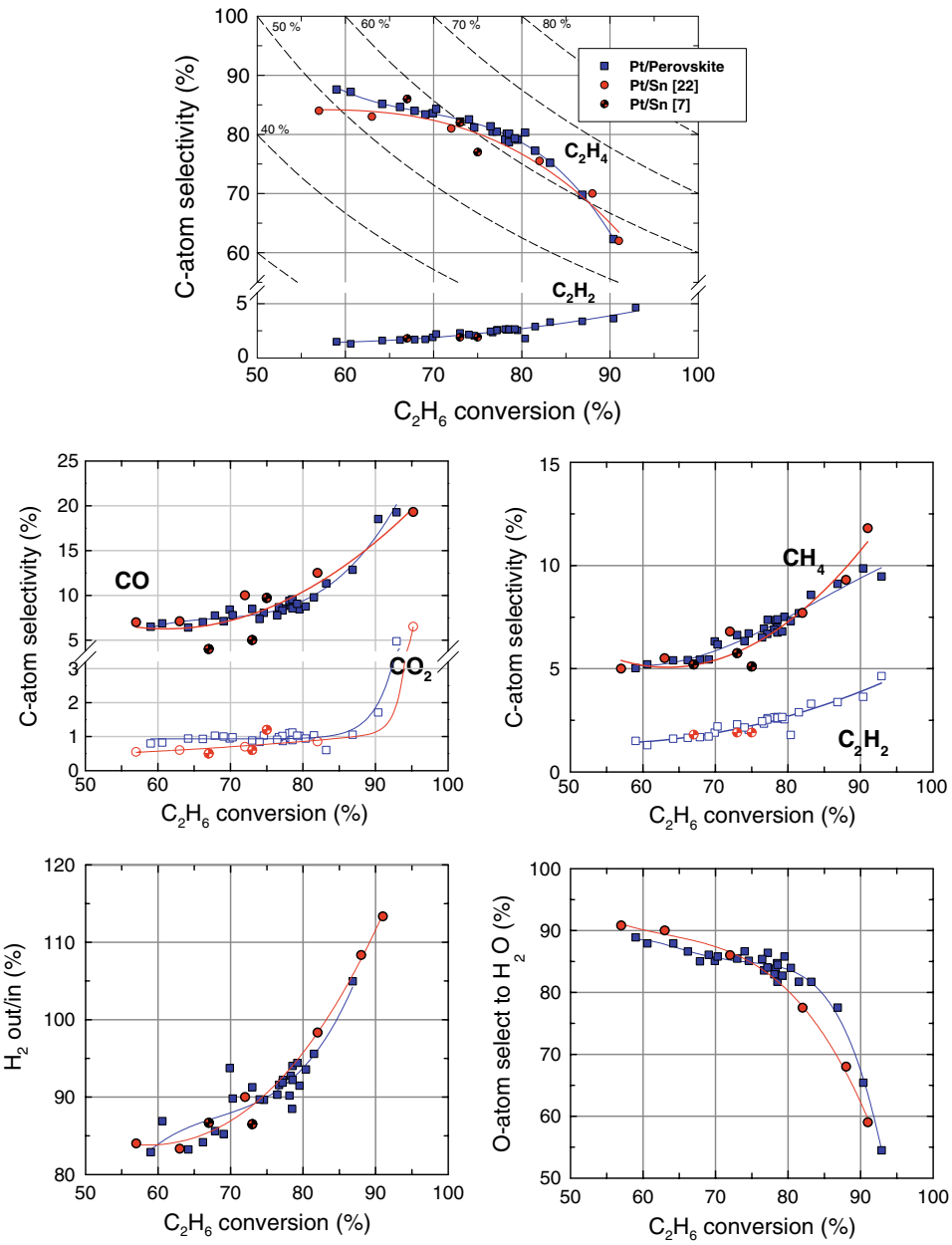

Fig. 4 Selectivity of the main products and ratio of H_2 produced and H_2 consumed as a function of ethane conversion during the CPO reaction on Pt–$LaMnO_3$ or Pt–Sn from literature data [7, 22]

ethane on the surface of Pt–$LaMnO_3$ catalyst. Since at the very high surface temperatures encountered in the ethane ODH H_2 oxidation is expected to be strongly in external diffusion limited regime, the enhanced selectivity to water appears to derive from a suppressed partial oxidation activity of Pt clusters strongly interacting with the perovskite sublayer.

Figure 4 shows that H_2 is consumed in the reactor on both Pt–$LaMnO_3$ and Pt–Sn catalysts at the same extent except at the highest process severity. Panuccio and Schmidt noted the economical drawback deriving from a net consumption of hydrogen at the conditions under which the selectivities of ethylene and other olefins are maximized ($H_2/O_2 = 3/1$) [23]. Considering the cost of H_2 make-up and in view of process economics it would be useful to place a WGS unit downstream of the ODH in order to close the H_2 balance recycling it after recover from the product stream rich of water and CO.

3.3 Contribution of Homogeneous Dehydrogenation

The observations described above strongly support the paramount importance of the catalyst for improving ethylene yield through its role of igniter of the feed mixture which is heated at the expenses of part of the fuel converted preferably to total oxidation products H_2O and CO_2 rather than

CO and H_2, in order to sustain the thermal (homogeneous) dehydrogenation of the remaining ethane to ethylene.

Some authors claim that the process can be represented by a two-zone model: in the first zone oxygen is depleted in the reaction with the sacrificial fuel, that is a fraction of ethane for C_2H_6/O_2 feeds or mostly hydrogen for $C_2H_6/H_2/O_2$ feeds, producing heat that sustains the following endothermic dehydrogenation of the residual ethane in the second zone. In particular, the first zone is catalytic, while the second zone is mainly in the gas phase [7].

Our previous studies by means of a 2-D model [8] showed a more effective sketch is obtained by a three-zone model, where the first zone is purely heterogeneous, with the consumption of oxygen and a fraction of the fuel until the onset temperature of the gas-phase dehydrogenation reaction is reached. The second zone is a hetero-homogeneous zone, where oxygen still reacts on the catalyst surface with the fuel to total oxidation products, but the fuel also reacts in the gas phase to dehydrogenation products through oxidative and non-oxidative reaction paths. The third zone begins when all of the oxygen is depleted and only endothermic gas phase reactions of dehydrogenation and pyrolysis take place.

This basically means that the great difference resides in the first and second zone of the three-zone model, where the catalyst actively participate to the reaction and where its contribution can be tuned by controlling its formulation and through the operating parameters.

In order to confirm such hypothesis all experimental data recorded on the Pt–$LaMnO_3$ system were reprocessed as suggested by Lange et al. [11] by plotting the C-atom selectivity (based on hydrocarbon products only) against the "cracking conversion" (Fig. 5), which was defined as

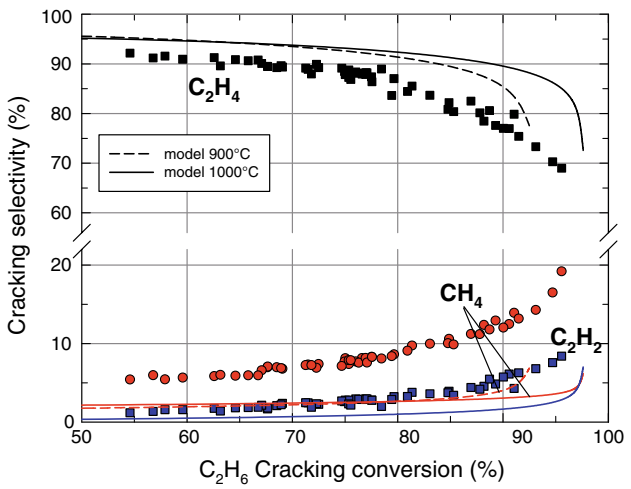

Fig. 5 C-atom "cracking selectivity" vs. "cracking conversion" obtained after normalization to exclude CO_x products. Lines represent the results predicted by the purely homogeneous steam cracking model in a plug flow reactor operated at 900 and 1,000 °C

the sum of all carbon minus unconverted ethane and CO_x. In fact, selectivities to main products (C_2H_4, CH_4, and C_2H_2) all follow narrow profiles, insensitive to the large range of experimental process conditions under which data were collected. In particular ethylene selectivity decreases with increasing 'cracking severity' as a consequence of clear increase in methane and, to a lower extent, C_2H_2 selectivity.

The experimental cracking selectivity profiles of Fig. 5 were compared with those relevant to such a final reactor zone, which, in first approximation was simply simulated by the Chemkin Plug code under isothermal conditions using the pure homogeneous kinetic scheme and considering an equimolar C_2H_6/H_2O mix.

Simulations of ethane steam thermal cracking at 900–1,000 °C predict the same observed experimental trend of products selectivities. In particular ethylene production trend is closely reproduced but slightly over predicted, whereas C_2H_2 and especially CH_4 formation are under predicted by the simplified isothermal steam cracking model. Similar discrepancies were also reported by Lange et al. who attributed them to the difference in temperature profile along the axial direction of the reactor: the real reactor operates with a temperature spike at the entrance of the catalyst bed followed by a continuous temperature decrease [11]. Hot spots are indeed notorious in decreasing the ethylene yields in steam crackers [2, 11].

In fact, simulations with a more complex hetero-homogeneous mechanism suggest that CH_4 is formed only at high temperatures at similar rates both in the gas phase and on the Pt surface when a large surface coverage of C and H is attained [24]. However the plug flow model is not accurate especially for CH_4 and C_2H_2 prediction, because local hot spots formed on the catalyst walls in the radial direction, which promote the formation of such species, are not captured. Indeed it was shown, from the comparison between mass-averaged temperature, conversion, and yield profiles of an adiabatic channel for a boundary-layer model and plug-flow model, the small differences that were observed to persist pertained especially to CO, CH_4, and C_2H_2 yields, which are higher in the 2D model [24].

CH_4 formation might be reduced by improving heat exchange between the catalytic surface and the gas phase, thus reducing the extent of hot spot formation. For instance, the reduction of pore size might be helpful in this task [25] as well as an increment in the thermal conductivity of the support.

Velocys Inc. has recently demonstrated [26] performance improvements associated to less steep temperature profiles, which can be obtained with a more complex heat management in microchannel reactors on stacked metal-plates.

4 Conclusion

The optimization of the performance of the Pt–$LaMnO_3$ catalytic system was carried out by means of an extensive experimental campaign devoted to investigate the main process tuning parameters, such as the C_2H_6/O_2 and H_2/O_2 feed ratios, space velocity and preheating temperature. Since the roles played by these parameters on ethane conversion and ethylene selectivity are coupled to each other, a simplified statistical analysis was employed to single out any effect of the main variables. By means of a linearized model it was found that any of the parameters showed an opposite impact on conversion and selectivity: when increased, C_2H_6/O_2 ratio, H_2/O_2 ratio, and space velocity reduce conversion and enhance selectivity while preheating temperature exhibits an opposite feature.

The performance achieved under optimized operating conditions over the novel Pt–$LaMnO_3$ catalyst, with a total molar yield to ethylene and acetylene in excess of 66% per pass, in correspondence to a C-atom selectivity to ethylene and ethane conversion both above 80%, is significantly better than our previous results and better than the best results reported in literature. Moreover, the reported data also highlight the high reproducibility of the performance of the catalytic system used and its great robustness, especially in the field of operation of greater interest for industrial application, where yields above 60% and selectivities above 80% were reached by means of different combination of C_2H_6/O_2 and H_2/O_2 feed ratios, space velocity, and preheat. The enhanced performance is mainly due to the more favorable product distribution, with higher selectivity to total oxidation species (CO_2 and H_2O), thus realizing a better heat management in the reactor.

A simplified homogeneous model of the post-catalytic zone, where the sacrificial fuel is already consumed, confirmed that most of ethylene is produced according to a homogeneous mechanism also in the case of Pt–$LaMnO_3$ system, depending mainly on the temperature attained in the reactor. Ethylene selectivity can be enhanced further by reducing side reactions (homogeneous and heterogeneous) of ethylene degradation, leading to C_2H_2 and CH_4, due to the presence of radial and axial hot spots along the reactor.

Acknowledgments The authors thank Mr. Vitale Stanzione for the experimental campaign. The financial support of Snamprogetti SpA is kindly acknowledged.

References

1. Sanfilippo D, Miracca I (2006) Catal Today 111(1–2):133
2. Kirk-Othmer (1978) Encyclopedia of chemical technology, 3rd edn. John Wiley & Sons, New York
3. Huff M, Schmidt LD (1993) J Phys Chem 97:11815
4. Huff M, Schmidt LD (1994) Catal Today 21:443
5. Schmidt LD, Huff M, Bharadwaj SS (1994) Chem Eng Sci 49(24A):3981
6. Bodke AS, Olschki DA, Schmidt LD, Ranzi E (1999) Science 285:712
7. Bodke AS, Henning D, Schmidt LD, Bharadwaj SS, Maj JJ, Siddall J (2000) J Catal 191:62
8. Donsì F, Caputo T, Di Benedetto A, Pirone R, Russo G (2004) AIChE J 50(9):2233
9. Chemsystems Nexant. PERP Report 03/04S2 (2004)
10. Ren T, Patel M, Blok K (2006) Energy 31:425
11. Lange J-P, Schoonebeek RJ, Mercera PDL, van Breukelen FW (2005) Appl Catal A: Gen 283:243
12. Schmidt LD, Siddall J, Bearden M (2000) AIChE J 46(8):1492
13. Lødeng R, Lindvåg OA, Kvisle S, Reier-Nielsen H, Holmen A (1999) Appl Catal A 187:25
14. Yokoyama C, Bharadwaj SS, Schmidt LD (1996) Catal Lett 38:181
15. US patent 6,846,773 (2005)
16. Cavani F, Ballarini N, Cericola A. (2007) Catal Today 127:113
17. Donsì F, Cimino S Pirone R, Russo G, Sanfilippo D (2005) Catal Today 106:72
18. Donsì F, Pirone R, Russo G (2002) J Catal 209(1):51
19. Donsì F, Cimino S, Pirone R, Russo G (2005) Ind Eng Chem Res 44(2):285
20. Cimino S, Donsì F, Pirone R, Russo G (2004) PCT WO 2004/105937A1
21. Kee RJ, Rupley FM, Meeks E, Miller JA Chemkin III: A Fortran package for the analysis of gas-phase chemical and plasma kinetics. Sandia National Laboratories Report SAND96–8216, Albuquerque, NM
22. Silberova B, Fathi M, Holmen A (2004) Appl Catal A: Gen 276:17
23. Panuccio GJ, Schmidt LD (2006) Appl Catal A: Gen 313:63
24. Donsì F, Williams KA, Schmidt LD (2006) Ind Eng Chem.Res 44(10):3453
25. Donsì F, Cimino S, Di Benedetto A, Pirone R, Russo G (2005) Catal Today 105(3–4):551
26. Long R, Daly F, Glass A, LaPlante T, Yuschak T, Mazanec T (2007) 20th NAM, Huston